Talanta 234 (2021) 122644

Contents lists available at ScienceDirect

Talanta

journal homepage: www.elsevier.com/locate/talanta

Selective point-of-care detection of pathogenic bacteria using sialic acid functionalized gold nanoparticles

Guillermo Landa [a,b], Laura G. Miranda-Calderon [a,b], Victor Sebastian [a,b,c,d], Silvia Irusta [a,b,c,d], Gracia Mendoza [c,d], Manuel Arruebo [a,b,c,d,*]

[a] Instituto de Nanociencia y Materiales de Aragón (INMA), CSIC-Universidad de Zaragoza, Zaragoza, 50009, Spain
[b] Department of Chemical Engineering, University of Zaragoza, Campus Río Ebro - Edificio I+D, C/ Poeta Mariano Esquillor S/N, 50018, Zaragoza, Spain
[c] Aragon Health Research Institute (IIS Aragon), 50009, Zaragoza, Spain
[d] Networking Research Center on Bioengineering, Biomaterials and Nanomedicine, CIBER-BBN, 28029, Madrid, Spain

ARTICLE INFO

Keywords:
Antimicrobial discrimination tests
Bacteria
MRSA
Gold nanoparticles
Biosensor
Staphylococcus aureus

ABSTRACT

In resource-limited settings, fast and simple point-of-need tests should facilitate healthcare providers the identification of pathogens avoiding empirical suboptimal treatments with broad-spectrum antibiotics. A rapid optical whole cell bacterial biosensor has been here developed using sialic acid functionalized gold nanoparticles allowing the selective screening of Gram-positive *Staphylococcus aureus* ATCC 25923 and Methicillin Resistant *Staphylococcus aureus* (MRSA) USA300 and Gram-negative bacteria (*Pseudomonas aeruginosa* ATCC 15442) by selecting the appropriate dispersing media. Those bacteria were selected due to their common presence in wound bed tissue of chronic infected topical wounds. The discrimination of bacterial pathogens has been attempted in different media including water, two independent buffers, bacterial broth, human serum and human urine. The identification of Gram + bacterial pathogens was also assessed under simultaneous co-culture of *S. Aureus* and *Pseudomonas aeruginosa*. High bacterial loads were required to provide with a statistically significant optical pathogen identification in human serum whereas it was not possible to detect the presence of bacteria at clinically relevant levels in urine.

1. Introduction

In the diagnosis and treatment of infectious diseases different bacterial identification tests are carried out in clinical microbiology laboratories using culture-based techniques (e.g., disk diffusion method, agar dilution testing, broth microdilution, Gram-staining, chromogenic screening plates, etc.) and automated techniques such as Matrix-Assisted Laser Desorption Ionization-Time of Flight Mass Spectrometry (MADI-TOF MS), polymerase chain reaction (PCR), enzyme linked immunosorbent assay (ELISA), DNA microarrays, DNA chips, loop-mediated isothermal amplification (LAMP), etc. [1,2]. Due to the time-consuming character of culture-based techniques or due to the high cost and requirement for a specialized training in the automated and genotypic methods, many of those techniques are therefore not amenable for point-of-care testing. Hence, it is of paramount importance the development of multiplexed (i.e., able to analyze multiple pathogens at once) point-of-care diagnostics to provide the healthcare practitioner with the identification of disease-causing pathogens to select the most appropriate antibiotic treatment. Those point-of-care (PoC) devices facilitate the access to physicians to rapid tests to discriminate between Gram+ and Gram- pathogens avoiding starting an empirical treatment with a suboptimal broad-spectrum antibiotic.

The most common point-of-care biosensors for the screening of bacterial infections and in some cases to also provide antimicrobial susceptibility tests are immunochromatographic lateral flow biosensors, molecular diagnostic systems, microfluidic platforms and nanotechnology-based approaches. Nano-based approaches include fluorescent, magnetic, metallic nanoparticles (NPs) or nanostructured surfaces (generally based on plasmonics) functionalized with selective recognition moieties (i.e., antibodies, aptamers, bacterial toxins, peptides, antibiotics, etc.). For instance, Gao et al. [3] described the sensible (10 CFU (colony forming units) per mL) detection in less than 2 h of bacteria in human blood by using magnetic NPs combined with a conjugated complex based on vancomycin and fluorescein. In that work vancomycin was used to generate multiple ligand-receptor interactions with the bacterial wall and the magnetic NPs were used to concentrate

* Corresponding author. Instituto de Nanociencia y Materiales de Aragón (INMA), CSIC-Universidad de Zaragoza, Zaragoza, 50009, Spain.
E-mail address: arruebom@unizar.es (M. Arruebo).

https://doi.org/10.1016/j.talanta.2021.122644
Received 22 February 2021; Received in revised form 4 June 2021; Accepted 18 June 2021
Available online 25 June 2021

the bacteria present in whole blood. Fluorescence resonance energy transfer (FRET) has been used to conjugate aptamer-functionalized gold NPs (used as acceptors) with upconversion nanoparticles (UCNPs) (used as donors) conjugated with the corresponding complementary DNA [4]. In the absence of bacteria, the UCNPs emission is quenched by the gold NPs absorption, whereas when bacteria are present the aptamers preferentially bind to bacteria and the fluorescence is restored reaching a detection limit as low as 3 CFU/mL. Luminescent UCNPs conjugated to magnetic NPs and to different selective aptamer sequences have also been used for the concentration and multiplexed detection of specific bacteria in complex samples reaching detection limits as low as 25, 10, and 15 CFU/mL for *S. aureus*, *Vibrio parahaemolyticus*, and *Salmonella Typhimurium*, respectively [5]. Immunochromatographic strips having antibody functionalized gold NPs have been used for the detection of whole-cell antigens against *Pseudomonas aeruginosa* and *S. aureus* simultaneously reaching detection limits within the 500–5000 CFU/mL range using a portable color intensity identifier [6]. A naked eye optical bacteria detection based on an isothermal RNA amplification reaction has also been carried out by functionalizing gold NPs with thiolated DNA probe conjugates using a sandwich hybridization reaction on nitrocellulose strips and the optical signal read in a scan software pre-installed in Android-based smart phones [7]. Using the device, a detection limit of 20 CFU/mL for *Listeria monocytogenes* from real milk and cheese samples was reached. A rapid visual detection of spirochaete bacteria (*Leptospira*) has been carried out by using multiplexed LAMP label-based lateral flow dipsticks using gold NPs coupled with anti-fluorescein antibodies [8]. Ligand-free gold NPs have been used to aggregate with different bacteria depending on their surface morphology providing distinctive optical readouts with a conventional spectrophotometer using the classical linear discriminant analysis [9]. In this case, positively charged gold nanostars were able to identify selectively ocular pathogens depending on their varied morphology, surface area and charge.

Not only the selective discrimination of pathogenic bacteria can be carried out using nano-based approaches, but also different NPs have aided in the assessment of antimicrobial susceptibility. In this regard, dextran-coated gold NPs have been conjugated to concanavalin A, which is carbohydrate-binding protein that aggregate bacteria, and depending on the bacterial metabolic state a shift in the surface plasmon band of the NPs was observed [10]. This concept was exploited in the high-throughput determination of antimicrobial susceptibility using those NPs to discriminate between inhibitory or non-inhibitory cohorts of *Escherichia coli* against ampicillin using a conventional microplate reader. The aggregation of Poly-L-lysine (PLL) functionalized gold NPs has also been used to evaluate the *Leuconostoc mesenteroides* NRRL B640 reduction in the bacterial cell numbers after nisin treatment [11]. In that work bacterial cell numbers as low as 10 CFU/mL could be quantified by measuring the extent of NPs aggregation and the unbound fraction of PLL. Also LSPR-based biosensors containing gold nanoparticles have been used to perform susceptibility sensing as an alternative to conventional Kirby-Bauer disk diffusion tests [12]. Aptamer-functionalized magnetic nanoparticles have also been used for bacteria capture combined with resistivity based detection to test bacteria directly for their susceptibility to antibiotics [13]. Surface-enhanced Raman scattering (SERS) biosensors based on nanoparticles surface functionalized with antibodies, aptamers, reporters, etc. have been widely used for antibiotic susceptibility testing [14].

S. aureus is a ubiquitous opportunistic pathogenic anaerobic Gram+ bacterium present in both community-acquired and nosocomial infections (e.g., implant-associated infections, endocarditis, osteomyelitis, septic arthritis and sepsis). MRSA is classified in the WHO list as a pathogen of the *high priority group* against which novel or repurposed antibiotics are urgently required. To limit the spread of MRSA and to provide with a fast and adequate antibiotic response to high risk patients with bacteremia, a rapid detection of the pathogen present and, ideally, the antibiotic susceptibility profile of its resistant phenotype are urgently needed.

Herein, we have functionalized gold NPs with *N*-acetylneuraminic acid, the predominant sialic acid (SA) found in human cells present as a terminal sugar on several glycoproteins, glycolipids and proteoglycans, to take advantage of the biogenic incorporation of SA by bacteria which use it as stealth monosaccharide to prevent immune recognition and as nutrient for cell wall synthesis [15]. Olson et al. [16] demonstrated using a genomic analysis that five different strains of *S. aureus* and three other species of *staphylococci* use *N*-acetylneuraminic acid as a carbon, nitrogen and energy source. To avoid immune recognition, Staphylococcal superantigen-like proteins, which depend on SA for their synthesis, bind to Toll-like receptors, which are responsible for the recognition of pathogens activating the production of proinflammatory cytokines and chemokines recruiting phagocytic macrophages [17]. Moreover, depending on the agglomeration state on the surface of the different bacteria, the surface plasmon resonance of gold NPs varied, being able to sense the presence of Gram+ and Gram- bacteria and to distinguish between a MRSA strain and a wild-type *S. aureus*. Poly (allylamine hydrochloride) (PAH) functionalized gold NPs were also included in the study as negative control to demonstrate the selective binding when using SA. PAH is a water soluble linear cationic polyelectrolyte with primary amine groups (free base types) which strongly electrostatically binds to negatively charged compounds.

The ability of this optical sensor to discriminate between an antibiotic resistant strain (MRSA) and wild type *S. aureus* was evaluated in water, two independent buffers, bacterial broth, human serum and human urine. The ability to discriminate in co-culture conditions of both Gram+ and Gram- bacteria was also assessed.

2. Materials and methods

2.1. Reagents

N-acetylneuraminic acid, sodium hydroxide, chloroauric acid ($HAuCl_4$), poly (allylamine hydrochloride) (PAH, MW 15,000 Da), sodium borohydride ($NaBH_4$), glutaraldehyde solution (50% wt. % in H_2O), phosphotungstic acid hydrate, osmium tetroxide solution (4% in H_2O) were purchased from Sigma-Aldrich (St. Louis, MO, USA). Tryptic Soy Agar (TSA) and Tryptic Soy Broth (TSB) were obtained from Conda-Pronadisa (Madrid, Spain). HEPES buffer solution (1 M) and Dulbecco's Phosphate buffered saline (DPBS; 1× and 10×) were purchased from Biowest (Cedex, France).

2.2. Gold nanoparticles synthesis

Gold nanoparticles (Au NPs) conjugated with *N*-acetylneuraminic acid (sialic acid, SA) were synthesized following a previously reported protocol [18]. In brief, 250 μL of an aqueous solution of 0.02 M $HAuCl_4$ were added to 10 mL of a 1.25 mM SA aqueous solution. The mixture was then stirred at 1,000 rpm and heated to 80 °C. Immediately after, 35 μL of 1 M NaOH were added and the reaction was continued for 15 min. The color of the solution changed from yellow to dark red, indicating the formation of Au NPs. Afterwards, the solution was cooled in an ice bath and the Au NPs were washed twice by centrifugation at 10,000 rpm using a Heraeus Megafuge 16 R centrifuge for 20 min. Then, the supernatant was removed, and the pellet was resuspended in DI water and maintained at 4 °C for further use.

Au NPs conjugated with PAH were synthesized as follows: 10 mL of a 0.25% (w/v) PAH solution was prepared in DI water and mixed with 200 μL of 0.1 M $HAuCl_4$, maintaining with mechanical stirring for 10 min. Next, 400 μL of 0.02 M $NaBH_4$ freshly-dissolved aqueous solution was added and then stirred for 45 min. The obtained red dispersion was cooled to room temperature and then washed twice by centrifugation at 12,000 rpm for 20 min. Then, the supernatant was removed, and the pellet resuspended in DI water and maintained at 4 °C for further use.

2.3. Nanoparticles characterization

Au NPs formation was monitored by UV–vis extinction spectroscopy. The analysis of the localized surface plasmon resonance from 400 to 700 nm was performed using a V-670 UV-VIS-NIR Jasco spectrophotometer. Zeta potential values for the colloidal suspensions of the Au NPs at neutral pH were obtained by using a Brookhaven 90plus particle size analyzer. The presence of the organic components (SA or PAH) on the surface of the Au NPs was evaluated by Fourier-transform infrared spectroscopy (FT-IR) using a VERTEX 70v FT-IR Spectrometer using an ATR Golden Gate accessory. Drops of functionalized NPs suspension were deposited on coverslips and dried at room temperature for IR measurements. Average size and morphology of the synthesized AuNPs were studied by TEM imaging. For the TEM sample preparation, 10 μL of the Au NPs were deposited on a carbon-coated copper grid (300 mesh, Electron Microscopy Sciences) and permitted to dry at room temperature. Ten microliters of a 3% (w/v) phosphotungstic acid hydrate in aqueous solution, negative staining agent, were added to the specimen to facilitate the observation of SA functionalization. TEM images were recorded on a FEI Tecnai T20 electron microscope operating at 200 kV. These images were then analyzed using ImageJ software to determine the morphology and size distribution of the Au NPs with a minimum of 200 nanoparticles measured. High-angle annular dark-field scanning transmission electron microscopy (HAADF-STEM) images were acquired using a high angle annular dark field detector in a FEI XFEG TITAN electron microscope operated at 300 kV equipped with a CETCOR Cs-probe corrector. Elemental analysis was carried out with an energy dispersive X-ray spectroscopy EDS (EDAX) detector which allows performing EDS experiments in the scanning mode. TGA analysis was used to quantify the amount of SA present on the surface of the AuNPs by monitoring the weight change that occurred after heating in air the SA functionalized AuNPs at a constant rate (10 °C/min) up to 600 °C using a Mettler Toledo TGA/SDTA 851 equipment.

2.4. Bacterial growth

Staphylococcus aureus ATCC 25923 (Ielab, Alicante, Spain) and the clinical strain Methicillin Resistant *Staphylococcus aureus* (MRSA) USA300 (kindly donated by Cristina Prat-Aymerich PhD, MD, at IGTP, Badalona, Spain) were selected as Gram-positive models. *Pseudomonas aeruginosa* ATCC 27853, also gifted by Dr Cristina Prat-Aymerich, was evaluated as a Gram-negative model. Bacteria liquid cultures were grown in TSB media overnight at 37 °C under stirring at 150 rpm, from inoculants to stationary growth phase (10^9 CFU/mL). Cells were harvested by centrifugation for 10 min at 4,000 rpm, washed in PBS (1×) and then resuspended in HEPES buffer (0.1 M) to reach a final cell density of 10^8 CFU/mL before further assays.

For the establishment of the co-culture of both bacteria, single colonies from *Staphylococcus aureus* ATCC 25923 and *Pseudomonas aeruginosa* ATCC 27853 were cultured in 4 mL of TSB for 24 h at 37 °C under stirring at 150 rpm to stationary growth phase (10^9 CFU/mL). Cultures were washed twice in PBS (1×), resuspended in HEPES buffer (0.1 M), diluted to reach 10^7 CFU/mL and mixed in a 1:1 proportion prior to further assays.

SA-AuNPs dispersion mass density after synthesis was determined by drying out 500 μL of the resulting suspension and weighting the dried residue in a MYA 5/2Y Radwag microbalance with 3 independent samples. To quantify the amount of SA present on the surface of the AuNPs, SA-AuNPs dispersion was lyophilized and thermogravimetric analysis was carried out by monitoring the weight loss after heating the sample in air at a constant rate (10 °C/min) up to 1000 °C using a Mettler Toledo TGA/SDTA 851 thermogravimetric analyzer.

2.5. Bactericidal evaluation assays

Minimum bactericidal concentration (MBC) and minimum inhibitory concentration (MIC) of de Au NPs were determined for *S. aureus* by the broth dilution method. Bacteria suspensions were prepared at a concentration of 10^5 CFU/mL in fresh TSB media containing serial concentrations of AuNPs (5, 10, 25, 50 and 100 μg/mL). After 24 h of incubation at 37 °C under shaking (150 rpm), cultures were diluted in PBS 1× in a 96-well microplate and then spot-plated into TSA plates. Grown bacterial colonies in plates were counted after 24 h of incubation at 37 °C. All measurements were made in triplicate and averaged. Samples not treated with AuNPs were used as positive control.

2.6. Bacterial detection assays

Human serum and urine samples and data from donors included in this study were provided by the Biobank of the Aragon Health System (BSSA, IACS) (PT17/0015/0039), integrated in the Spanish National Biobanks Network and they were processed following standard operating procedures with the appropriate approval from the Ethics and Scientific Committees of our University. The pH of urine samples was adjusted to three different values (4.5, 7.5 and 9) by adding acetic acid or sodium hydroxide in order to provide with different physiological backgrounds.

The assay for bacterial detection was performed in 96-well microplates. 20 μL of AuNPs suspensions were diluted in 160 μL of different media (water, DPBS, HEPES, TSB, human serum and human urine) to reach a final concentration of 50 μg/mL. This concentration was selected to provide with a strong optical signal with the naked eye after bacterial recognition. Then, 20 μL of the selected bacteria in HEPES buffer were added to the diluted Au NPs solutions to obtain a final concentration in the 10^5–10^7 CFU/mL range. Samples of diluted Au NPs (50 μg/mL) in the different media without adding bacteria were also tested as control. During the assay, the microplates were maintained at 37 °C with stirring at 150 rpm in order to facilitate the interaction of the bacteria with the Au NPs. All measurements were made twice for each concentration, averaged and repeated three times. UV–vis extinction spectroscopy analysis from 400 to 700 nm was performed using a in a microplate reader (Multimode Synergy HT Microplate Reader; Biotek, USA) at different time points (1, 2, 4, 8 and 24 h) to observe changes in the optical plasmon resonance spectra of the Au NPs.

Supramolecular interactions between bacteria and Au NPs were studied by scanning electron microscopy (SEM) and TEM. Various *S. aureus* suspensions (10^7 CFU/mL) were prepared in TSB media with Au NPs (50 μg/mL) and incubated during 1 h at 37 °C. Next, the bacteria treated with the AuNPs were washed 3 times at 3,000 rpm in PBS 0.1 M (10×) and finally resuspended and fixed with a 2.5% glutaraldehyde solution, in which samples were incubated for 2 h at room temperature. For the SEM sample preparation, bacteria were again washed as in the previous steps to get rid of the fixing agent and filtered onto a 0.2-μm polycarbonate filter. The filters were dehydrated through a graded ethanol series, dried at room temperature, deposited on a microscope slide and coated with carbon in a Leica EM ACE200 sputter coater as previously reported in our group [19]. SEM and electron backscatter diffraction (EBSD) images were obtained in a FEI Inspect F50 electron microscope.

For TEM sample preparation, same suspensions were centrifuged to obtain pellets composed of bacteria and the conjugated AuNPs. Pellets were stained for 1 h at room temperature using osmium tetroxide (1% v/v in water), dehydrated through a graded ethanol series, and embedded in epoxy resin. Ultrathin sections were cut with a diamond knife using a Leica EM UC7 ultramicrotome. TEM images were recorded on a FEI Tecnai T20 electron microscope operating at 200 kV.

2.7. Statistical analysis

Data statistical analysis was carried out using a 2-way ANOVA test followed up by a Dunnett's multiple comparison test with GraphPad Prism 7 software. Error bars represent mean plus standard deviation (*p

< 0.05, **p < 0.01, ***p < 0.001, ****p < 0.0001).

3. Results

Fig. 1a and b shows the morphology of the PAH-functionalized and SA-functionalized AuNPs used in this work. The insets in Fig. 1a and b depict the stained organic layer of PAH and SA, respectively present on the surface of the Au NPs. Particle size analysis of the resulting particles shows a Gaussian distribution with maxima at 12 and 20 nm for the PAH-AuNPs and SA-AuNPs, respectively (Fig. 1c). The Zeta potential values measured at neutral pH were 10.13 ± 1.56 mV for PAH-AuNPs and −13.21 ± 1.87 mV for SA-AuNPs. Both colloidal suspensions showed a surface plasmon resonance (SPR) absorption maximum centered at 520 nm (Fig. 1d). According to the FTIR analysis (Fig. 1e) both one-pot synthesis methods produced Au NPs sharing the characteristic SA and PAH bands present in those functional molecules. The absorbance peaks were weaker and broader in Au functionalized spectra compare to the pure organic molecules due to the lower concentration of these compounds present in the samples as commonly reported [20]. For the PAH-AuNPs the characteristic band at 1603 cm^{-1} related to the in plane *N*–H bending of the organic molecule can be observed as a shoulder on the band attributed to the O–H bending of the remaining adsorbed water [21]. In this range the asymmetric vibration of the *N*–H group and a peak assigned to the C–H bending (1387 cm^{-1}) could also be observed. Overlapped to the broad band due to the O–H stretching of adsorbed water, two weak signals at 2926 and 2865 cm^{-1} confirm the presence of PAH on the surface of the NPs [22,23]. The IR spectrum of SA-AuNPs shows the characteristic adsorption stretching band of amide group and hydroxyl group in the region 3600-2900 cm^{-1} and peaks at 2917 and 2850 cm^{-1} that would be related to the C–H stretching [24]. Broad bands are observed in the region assigned to the amide I and amide II stretching vibrations (1690–1590 and 1500-1580 cm^{-1}, respectively). On the other hand, peaks at 1754 and 1722 cm^{-1} associated to ester carbonyl stretching modes are extremely weak and shifted to lower wavenumbers suggesting hydrogen bonding interactions as reported in the literature [25]. A broad band can be also observed in the 100-1500 cm^{-1} region due to SA C–O and C–OH stretching [26]. Thermogravimetric analysis of the SA-AuNPs (Supplementary material, Fig. S1a) revealed that after the degradation of the organic compound the remaining mass of gold represents 71.5 wt%, which implies a 28.5 wt% of SA. The analysis of the UV–vis spectrum for the SA and SA-AuNPs from 190 nm to 700 nm (Fig. S1 b,c) revealed that only a 7.8 wt% of the SA incorporated in the synthesis as precursor remained on the final SA-AuNPs dispersion, representing a 27.9 wt% of the final material in good agreement with the TGA results.

The colorimetric analysis of the interaction between SA-AuNPs or PAH-AuNPs and the three bacteria analyzed (*S. aureus*, MRSA and *P. aeruginosa*) in different media is depicted in Fig. 2. The quantification of the UV–vis absorbance ratio at 600 and 520 nm is used to statistically analyze the agglomeration state of Au-NPs under the presence of bacteria. At 600 nm the absorption of the culture media is despicable and the changes in the optical density can be attributed to the growth of a bacterial population. By subtracting from the signal of the Au-NPs with bacteria the signal of the medium with the bacteria without Au-NPs we could obtain the agglomeration state of the Au NPs. When using PAH-AuNPs (Fig. 2a) statistically significant results were obtained in the identification of the presence of 10^7 CFU/mL bacteria in water, PBS and HEPES but when using a complex media (i.e., TSB, a soybean-casein digest medium) the nanoparticles failed in detecting the presence or absence of bacteria. However, when using SA-AuNPs, the detection of pathogenic *S. aureus* and MRSA was possible and, more importantly, distinct signals for MRSA and for wild-type *S. aureus* were obtained in TSB (Fig. 2 b-e) being possible to identify the presence of Gram+ bacteria even with the naked eye (Fig. 2 c). With the naked eye we were able to see that when adding the sialic acid coated nanoparticles to Gram- bacteria (*P. Aeruginosa*) the characteristic culture medium color (pink)

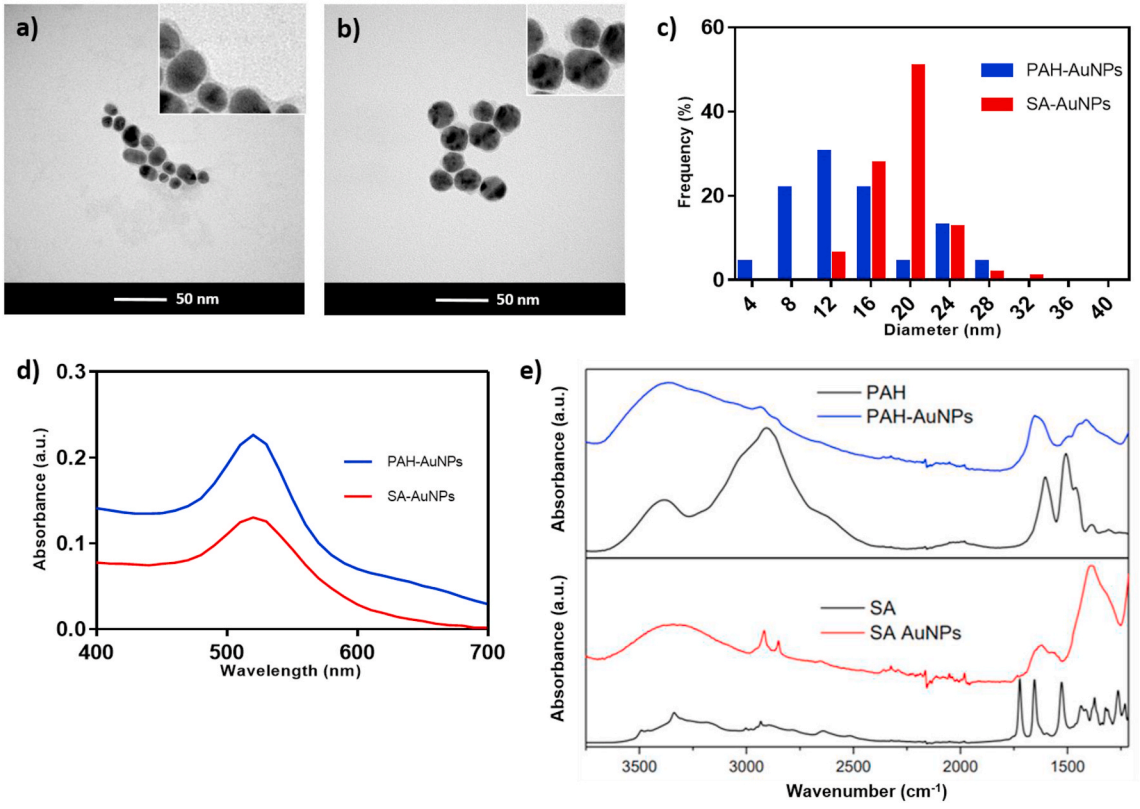

Fig. 1. AuNPs characterization. a) and b) TEM images of PAH-AuNPs and SA-AuNPs, respectively. Insets, high magnification image to show the stained organic coating on the surface of AuNPs c) Size distribution of AuNPs. d) Absorption spectra of AuNPs. e) FT-IR of AuNPs, PAH and SA.

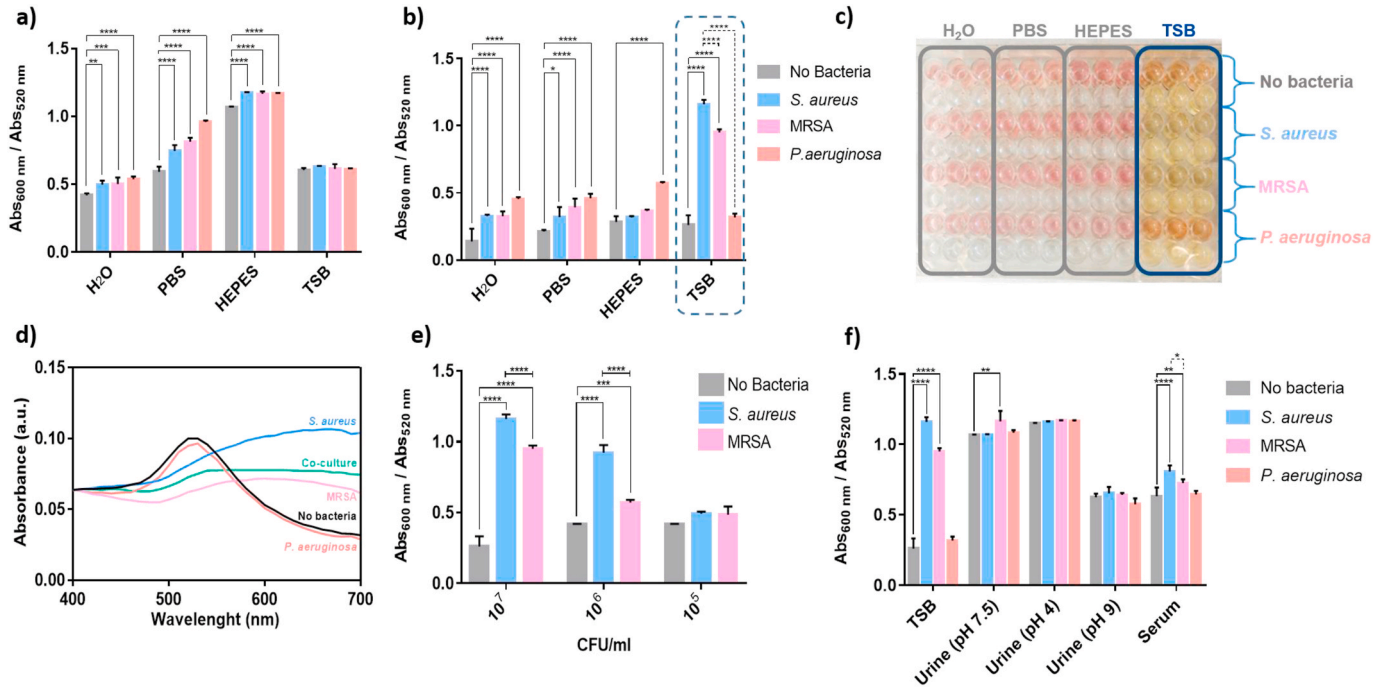

Fig. 2. Response of AuNPs to the presence of bacteria. a) and b) Abs 600/Abs 520 nm ratio for PAH-AuNPs and SA-AuNPs, respectively in the presence of different bacteria in various media. Error bars represent the standard deviation of the mean (*p < 0.05, **p < 0.01, ***p < 0.001, ****p < 0.0001). TSB incubation data obtained from SA-AuNPs and statistical differences between *S. aureus* and the rest of bacteria are highlighted with a dashed line. c) and d) Change in colour and absorption spectra of the SA-AuNPs in presence of bacteria. In Figure c for each bacteria the first row shows the optical signal of the medium containing the nanoparticles and the second row depicts the color observed in the absence of nanoparticles. e) Abs 600/Abs 520 nm ratio of SA-AuNPs against different concentrations of *S. aureus* and MRSA. f) Abs 600/Abs 520 nm ratio of SA-AuNPs in presence of bacteria using human urine as dispersive medium. (For interpretation of the references to color in this figure legend, the reader is referred to the Web version of this article.)

did not change but when adding them to Gram+ bacteria (either MRSA or wild type *S. Aureus*) the color turned into yellow. The absorbance spectra for pristine SA-AuNPs and for the SA-AuNPs under the presence of wild type *S. aureus*, MRSA and *P. aeruginosa* in TSB after background subtraction of the signal of the free bacteria in TSB is shown in Fig. 2d. The sharp SPR peak at 520 nm for the pristine NPs red-shifted to become a broad peak along the VIS spectrum which indicates nanoparticle agglomeration due to the reduction in the interparticle spacing and scattering increase. This effect can be attributed to the bacterial incorporation of sialic acid as a nutrient for cell wall synthesis as we mentioned before due to the presence of specific transporters on the cell wall which would uptake those SA-functionalized gold nanoparticles promoting the reduction in the interparticle spacing and scattering increase. The identification was also carried out under co-culture conditions of *Staphylococcus aureus* and *Pseudomonas aeruginosa* (Fig. 2d and Fig. S1d) showing a clear absorbance peak characteristic of SA-AuNPs agglomeration even under the presence of Gram- bacteria. The statistical analysis of the A_{600}/A_{520} ratio with increased concentrations of bacteria present could be used (Fig. 2e) to identify the presence of bacteria even in serum and also to perform a susceptibility test due to the distinct signals observed for the MRSA and for the wild type *S. aureus*. Statistical significance in the detection was observed for bacterial loads $\geq 10^6$ CFU/mL. Therefore, we were able to discriminate signals above that threshold with 1-log sensitivity. Fig. 2f shows that while in TSB sialic-acid functionalized gold nanoparticles are able to discriminate Gram+ from Gram- bacteria and between MRSA and wild type *S. aureus* (10^7 CFU/mL), those bacterial loads were not detected in human urine at any of the pHs tested. This could be attributed to the presence of urea in the urine and its ability to break hydrogen bond interactions in host-guest chemistry [27]. As we mentioned before, *S. aureus* use different enzymes (e.g., *N*-Acetylneuraminate lyase) to degrade sialic acid as a source of carbon, nitrogen and energy. Hydrogen bonds have been identified as responsible for enzyme/substrate binding between MRSA *N*-acetylneuraminate lyase and the 2 R-diastereoisomer of sialic acid [28]. Therefore, the binding ability of SA-functionalized Au nanoparticles would be impaired under the presence of a hydrogen bonding inhibitor (i.e., urea), corroborating the initial hypothesis that strong supramolecular interactions are responsible for the binding between SA-AuNPs and bacteria. In the same way, a 10^7 CFU/mL bacterial load was used to evaluate the efficacy of the developed formulations in human serum. Using a conventional minimally invasive blood withdrawal, serum can be easily separated by clotting and centrifugation. Even in the complexity of the serum composed of proteins monosaccharides, electrolytes, hormones, etc., we were able to statistically identify the presence of bacteria using the SA-AuNPs having a unique signal for both bacterial strains (Fig. 2f).

The interaction of SA-AuNPs with bacteria is shown in Fig. 3a–d where SEM images in secondary and backscattered electrons demonstrate that the surface of bacteria is decorated with clusters of agglomerated SA-AuNPs. The amount of gold nanoparticles decorating the surface of bacteria increased over time which induced agglomeration as corroborated with the wide absorption peak obtained during the bacterial detection (Fig. 2d). Ultrathin stained sections of SA-AuNPs and bacteria were obtained by ultramicrotomy and were analyzed by transmission electron microscopy. TEM images (Fig. 4 a-c) depict individual nanoparticles located on the bacteria membrane. Comparing the interaction after 10 min and 1 h of contact, it was observed that this interaction is time-dependent showing larger nanoparticle-based agglomerates over time. Back scattered SEM images (Fig. 3 b,d) and HAADF-STEM images (Fig. 4 d,e) corroborated the presence of the AuNPs due to the high brightness of Au atoms (high electronic density). The crystalline structure of Au NPs was preserved during the incubation with *S. aureus* (inset Fig. 4e). On the other hand, EDS analysis of nanoparticles located on the bacteria membrane confirmed the presence of Au nanoparticles (Fig. 4f), revealing the characteristic energies of Au X-Ray transitions together with the ones coming from the Cu microscopy

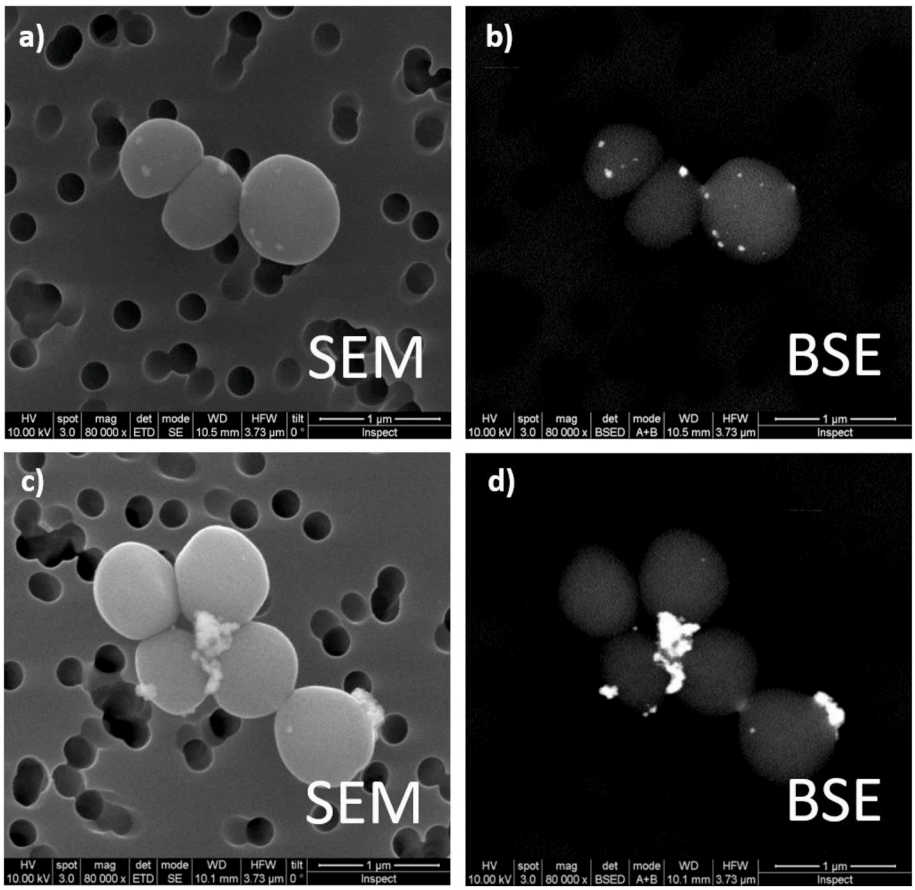

Fig. 3. SEM and EBDS images of *S. aureus* and after being incubated with SA-AuNPs in TSB for 10 min (a,b) and 1 h (c,d).

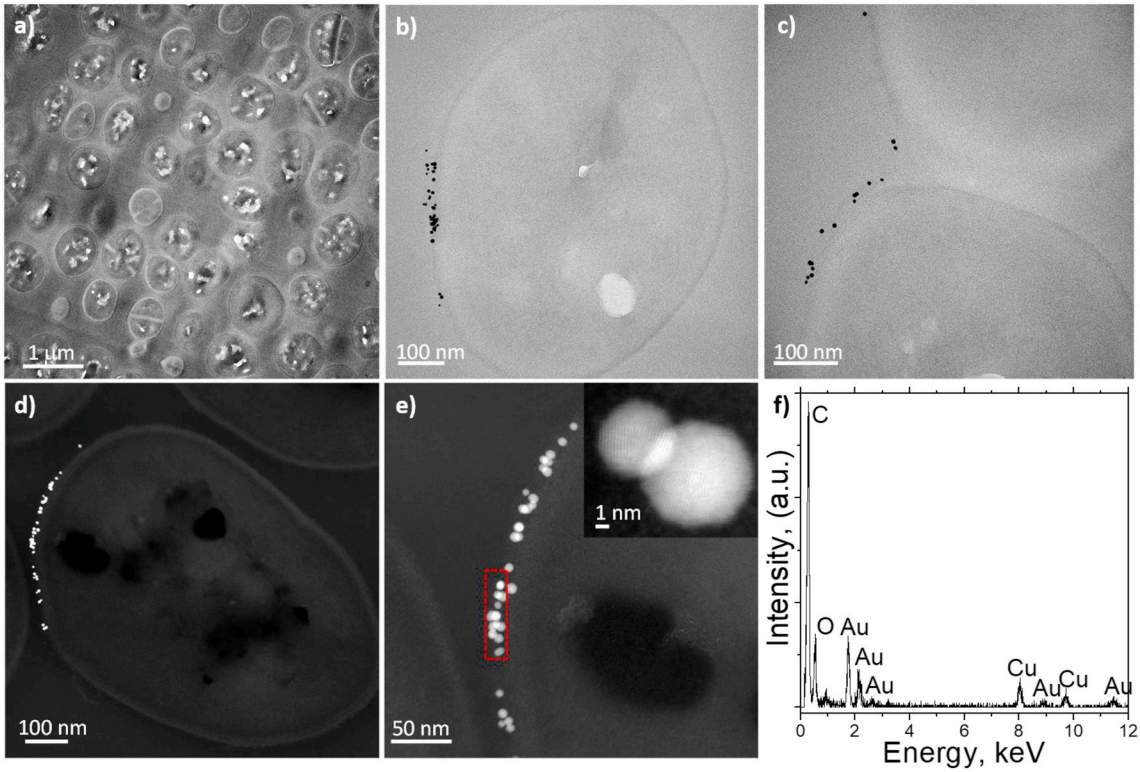

Fig. 4. Electron microscopy analysis of *S. aureus* after being incubated with SA-AuNPs. (a,b,c) TEM, (d,e) HAADF-STEM images and (f) EDS analysis of the red dashed area marked in (e). (For interpretation of the references to color in this figure legend, the reader is referred to the Web version of this article.)

grid used as support. Fig. 5 shows the supramolecular interactions based on electrostatic attraction between the negatively charged bacterial peptidoglycan layer and polysaccharide capsule and the positively charged PAH. The morphology of the bacteria was largely affected when using PAH-AuNPs compared to the preserved structure observed when using SA-AuNPs.

In order to address the possible effect of the Au NPs on the bacteria during colorimetric detection assays, bactericidal effects of SA-AuNPs and PAH-AuNPs were evaluated. MIC (defined as 2-log reduction in the visible growth of bacteria after overnight incubation at 37 °C) or MBC values for all bacteria were not reached even at the maximum dose of SA-AuNPs tested (100 μg/mL) (Fig. 6a). We also observed that the *S. aureus* growth depends on the culture media used and the stationary phase was reached at different cell counts (~10^9 CFU/mL in TSB and ~10^6 CFU/mL in serum) (Fig. 6c and d). Fig. 6b shows MIC and MBC values for *S. aureus* wild type, which were reached at 5 and 25 μg/mL of PAH-AuNPs, respectively. Those results agree with the altered morphology observed in Fig. 5 and could explain the incapability to detect the presence of bacteria in the colorimetric assays by using PAH in this formulation.

4. Discussion

The need of developing simple PoC sensors based on naked eye detection for discriminating MRSA and wild type *S. aureus* would be interesting in resource-limited settings in order to select the most appropriated antibiotic treatment. Herein, we have used Au NPs as colorimetric sensor to discriminate between Gram+ and Gram- bacteria and between MRSA and wild type *S. aureus* in different media. In this regard, we have prepared two different Au NPs having a positively charged polyelectrolyte (i.e., PAH) or sialic acid on their surfaces in order to take advantage of the preferential uptake of sialic acid by *S. aureus* as energy and carbon source. As we mentioned before, both colloidal gold-based suspensions showed a SPR absorption maximum centered at 520 nm. This dipolar oscillation in resonance with the irradiating light at a specific frequency depends on the particle size and shape. In our case, the sizes observed by TEM (12 and 20 nm for the PAH-AuNPs and SA-AuNPs, respectively) match the expected absorption maximum observed at 520 nm as previously reported for Au NPs in that size range [29]. Isolated colloidal Au nanoparticles absorb the VIS irradiating light by collective excitations of conduction electrons generating SPR, by electronic transitions from occupied to empty bulk energy bands and by the scattering of conduction electrons [30]. The later absorption is minimized for colloidal non-aggregated systems but when agglomeration or irreversible aggregation take place, scattering prevails over the other two mechanisms and a red-shift occurs towards higher wavelengths disappearing the Au NPs SPR. Electric dipole-dipole interactions and plasmon coupling of the neighboring particles forming the aggregate are responsible for this shift [18].

Lee et al. [31] used this aggregation-based concept to identify the presence of influenza virus in culture media using SA-AuNPs considering that virions attach to target cells by binding activated hemagglutinin to sialic acid receptors.

As it is shown in Fig. 3 AuNP agglomeration on the bacteria surface is a time dependent mechanism increasing over time. No NPs were found inside the bacteria which indicates that SA interacts with the bacteria cell wall probably following the endogenous incorporation of SA in different strains of *S. aureus* (including MRSA) using the chromosomal locus transporter (NanT gene) before starting to catabolize *N*-acetylneuraminic acid as carbon source [16]. It has been demonstrated that

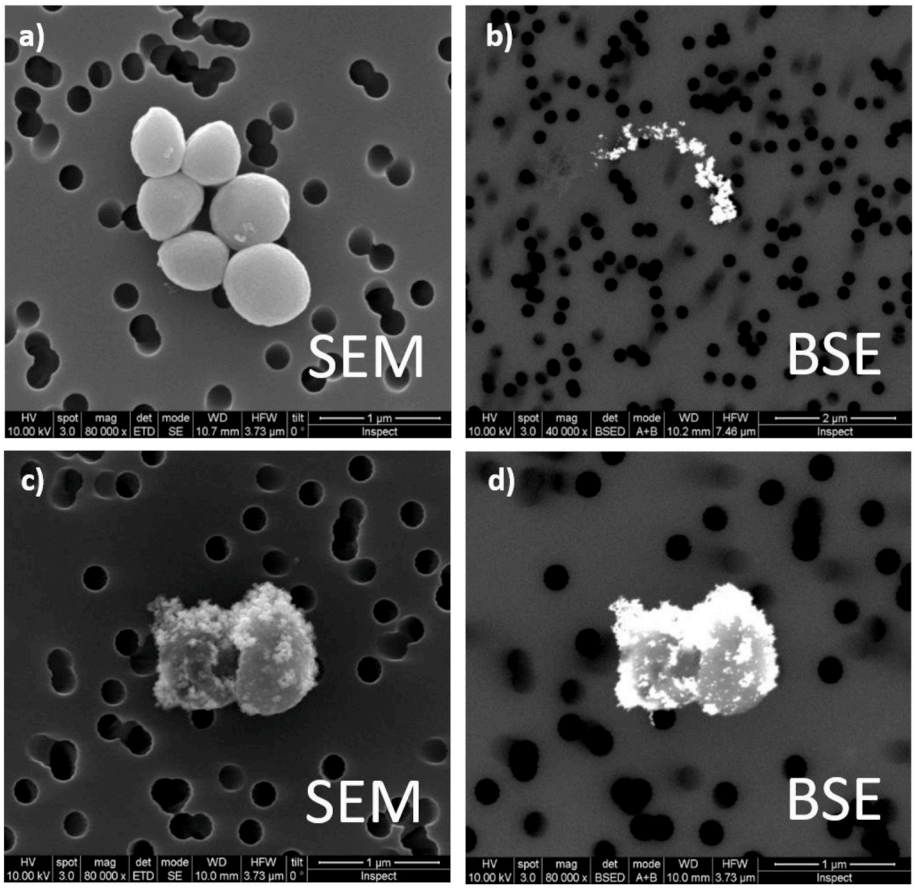

Fig. 5. SEM and EBDS images of *S. aureus* after being incubated with PAH-AuNPs in HEPES buffer. a) b) Unmatched *S. aureus* and PAH-AuNPs. c) d) Altered morphology *S. aureus* coated with PAH-AuNPs.

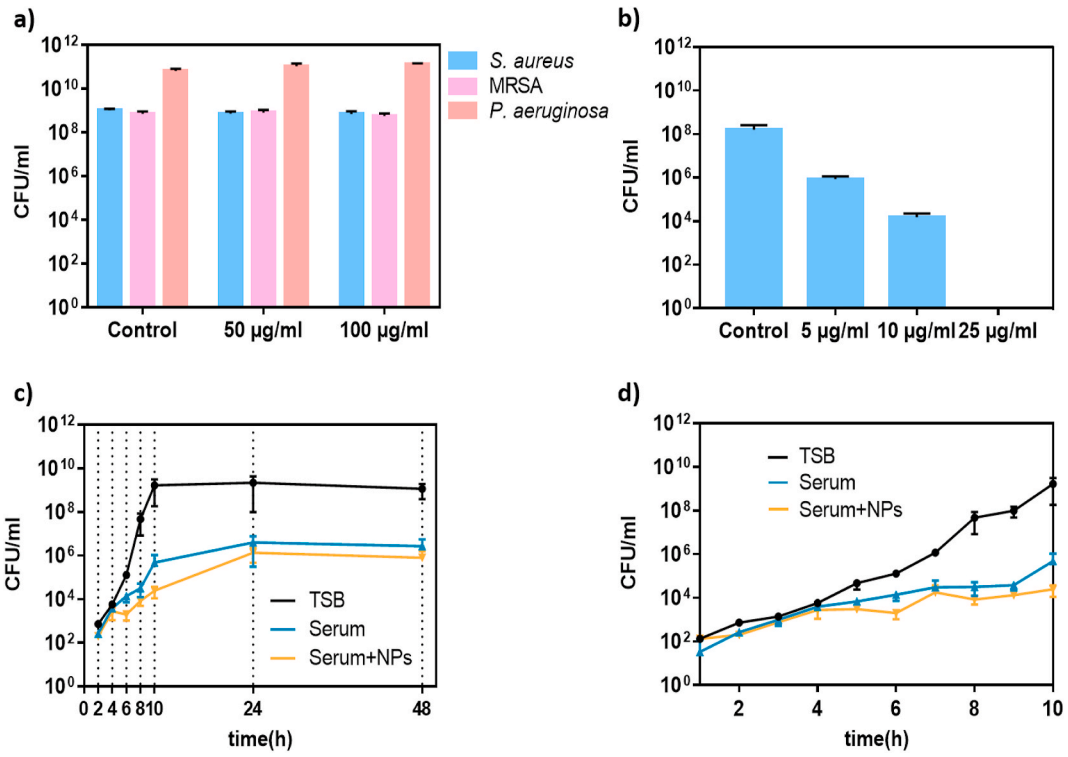

Fig. 6. a) Bactericidal action of SA-AuNPs against different bacteria. b) Bactericidal action of PAH-AuNPs against *S. aureus*. c) d) *S. aureus* growth kinetics in TSB and human serum in presence or absence of SA-AuNPs.

the *staphylococcal* murein sacculi are impermeable to proteins [32] therefore, it would be very unlikely that 20 nm in diameter Au NPs could cross the 20–40 nm thick peptidoglycan layer as we observed by electron microscopy images.

The colorimetric analysis showed in Fig. 2 revealed a concentration dependence for the optical test here developed. In this medium we were able to distinguish between Gram+ and Gram- bacteria (Fig. 2 b,c) and also statistical significance was obtained between the wild type and the MRSA (Fig. 2e). However, a limit of detection in TSB was reached for bacterial loads higher than 10^5 CFU/mL which are much higher than the common bacterial counts reached during bacteremia (>50 CFU/mL) [33,34]. In symptomatic urinary tract infections bacterial loads higher than 10^5 CFU per mL of urine are commonly used to diagnosis bacteriuria [35]. Therefore, both serum and urine were used as suspension media to evaluate the ability of the optical sensor here developed to detect bacteria. The different signals provided for the different bacterial strains could be used as an antibiotic susceptibility test in TSB after obtaining different signals for MRSA and S. Aureus wild type. This differences between strains could be attributed to the different envelope composition. Müller et al. [36] demonstrated that MRSA has a reduced peptidoglycan cross-linking compared to other *S. aureus* strains and this reduction induces a strong immune response and superior pathogenicity by making it resistant to intracellular degradation by immune cells. In addition, MRSA has also a different content in wall teichoic acids in its envelope than its wild type counterpart being those acids covalently linked to the peptidoglycans present on the bacterial cell wall [37].

We also observed that using SA-AuNPs the identification of the presence of the Gram- bacterium *P. aeruginosa* ATCC 15442 was only possible in water, PBS and HEPES, but failed in TSB, human serum and urine. Competitive adsorption of the different components present in TSB might be part responsible for this effect. *P. aeruginosa* also uptakes exogenous sialic acid in a time-dependent manner through a specific linkage improving its pathogenicity [38]. Nevertheless, the differences between the results obtained for *S. aureus* and *P. aeruginosa* could be attributed to the different nature of the outside of the outer membrane for Gram- bacteria, which is composed mainly of lipopolysaccharides surrounding an interior thin peptidoglycan cell wall, whereas Gram+ bacteria do not have an outer membrane but a thick peptidoglycan layer. The identification of *S. aureus* was independent on the presence of other bacteria which highlights the interest of the proposed system. In addition, different transporters of sialic acid have been identified for Gram+ and Gram- bacteria, having the later a protein-mediated transport across the outer membrane to the interior of the cell in addition to the common transport through porins which could explain the differences observed [39].

Previous works also managed to detect the presence of bacteria in clinical samples by monitoring the state of aggregation of Au NPs. For example, Yang et al. [40] used D-alanine-D-alanine surface functionalized gold nanoparticles. Relying on the bacterial uptake of the oligopeptide and measuring the red-shifting of the Au NPs optical spectrum, they were capable of detect the presence of different Gram + bacteria, achieving a limit of detection of 3.2×10^2 CFU/mL for S. aureus. While their method was robust in detecting the presence of bacteria in clinical samples, it was not suitable to discriminate between Gram+ and Gram- bacteria. In contrast, Zhu et al. [41] developed a rapid method for the identification of bacterial lipopolysaccharides (LPS) using gold nanoparticles functionalized with two different DNA aptamers. Au NPs functionalized with ethanolamine aptamer could bind to ethanolamine and recognize any type of LPS, causing the aggregation of the Au NPs with the bacteria and a color change from red to blue. In the same way, Au NPs functionalized with an aptamer against the LPS of *E. coli* O111:B4 specifically bond O111:B4 LPS and they were capable of discriminate between *E. coli* strains. With this two probes a typing method was developed, detecting LPS in concentrations between 2.5 and 20 µg mL^{-1}, with a detection limit of 1 µg mL^{-1}.

This strategy is not restricted to the use of Au NPs. Shin et al. [42] developed a colorimetric assay based on the aggregation of blue-colored polymeric nanobeads using vancomycin as ligand. When the functionalized nanobeads were incubated with Gram+ bacteria, the binding between the two caused the apparition of blue precipitates that were

visible with the naked eye, without any pre-processing steps. Using a porous filter system for collecting the precipitates, they achieved a limit of detection of 2.5×10^5 CFU μL^{-1} for Gram + bacteria whit incubation times under 30 min. Increasing the incubation times permitted the detection of concentrations as low as 3.1×10^4 CFU μL^{-1}.

In urine our sensor was unable to identify the presence of bacteria at the doses tested probably due to the disruption in the hydrogen bonding interaction between sialic acid and the bacteria due to the strong ability of urea to break hydrogen bond interactions in host-guest chemistry. The agglomeration and aggregation state of SA-AuNPs strongly depends on the dispersion media. We show that in TSB we have been able to develop a colorimetric sensor based on the preferential uptake of sialic acid by S. aureus. In serum we were still able to identify the presence of bacteria but the sensor failed in discriminating the two different strains studied.

5. Conclusions

The preferential uptake of sialic acid by pathogenic bacteria can be used to agglomerate gold nanoparticles on their surfaces whereas a conventional positively charged polyelectrolyte attached to the surface of the same nanoparticles was unable to discriminate bacteria. This optical sensor was developed by a simple colorimetric analysis of the SPR band in the visible region showing that under the presence of bacteria the sharp SPR absorbance peak at 520 nm for the pristine NPs red-shifted to become a broad peak along the VIS spectrum which indicates nanoparticle agglomeration due to the reduction in the interparticle spacing and scattering increase. The optical sensor here developed can also be used to discriminate between wild type *S. aureus* and MRSA which is one of the leading pathogens of hospital-acquired infections. The sensor was able to identify the presence of Gram+ bacteria even under co-culture conditions with other Gram- bacteria. The discrimination ability between Gram+ and Gram-bacteria can be attributed to the different nature of the outside of the outer membrane for Gram- bacteria which is composed mainly of lipopolysaccharides surrounding an interior thin peptidoglycan cell wall, whereas Gram+ bacteria do not have an outer membrane but a thick peptidoglycan layer, and also to the different transporters of sialic acid identified for both types of bacteria. While the sensor was able to perform identification under TSB medium and in serum samples, it failed to identify bacteriuria in urine, probably due to the disruption of the hydrogen bonding between sialic acid and bacteria due to the presence of urea.

Author contributions

Conceptualization, S.I. and M.A.; Data Curation, G.L, V·S, S·I, G.M. and M.A.; Formal Analysis, G.L, S·I, G.M. and M.A.; Funding Acquisition, S.I. and M.A.; Investigation, G.L. and L.M.; Methodology, G.L, L.M. and V·S.; Project administration: S·I, G.M. and M.A.; Resources, S.I. and M. A.; Software, G.L.; Supervision, V·S, S·I, G.M. and M.A.; Validation, S.I. and M.A.; Visualization G.L; Writing-Original Draft Preparation, G.L. and M.A.; Writing-Review and Editing, G.L, L.M, V·S, S·I, G.M. and M.A.; All authors have read and agreed to the published version of the manuscript.

Declaration of competing interest

The authors declare that they have no known competing financial interests or personal relationships that could have appeared to influence the work reported in this paper.

Acknowledgments

This research was funded by the Spanish Ministry of Economy and Competitiveness (grant number CTQ2014-52384-R). Financial support from the EU thanks to the ERC Consolidator Grant program (ERC-2013-CoG-614715, NANOHEDONISM) is also acknowledged. G.L. acknowledges the support from the FPI fellowship PRE2018-085769 granted by the Spanish Ministry of Science, Innovation and Universities, while L.G.M-C. acknowledges the financial support from the Mexican Council of Science and Technology (CONACyT) through doctoral grant#710618. G.M. gratefully acknowledges the support from the Miguel Servet Program (MS19/00092; Instituto de Salud Carlos III). VS acknowledges the LMA-INA for offering access to their instruments and the financial support of Ministerio de Ciencia, Innovación y Universidades, Programa Retos Investigación, Proyecto REF: RTI2018-099019-A-I00. CIBER-BBN is an initiative funded by the VI National R&D&i Plan 2008–2011, Iniciativa Ingenio 2010, Consolider Program, CIBER Actions and financed by the Instituto de Salud Carlos III (Spain) with assistance from the European Regional Development Fund.

Appendix A. Supplementary data

Supplementary data to this article can be found online at https://doi.org/10.1016/j.talanta.2021.122644.

References

[1] H. Leonard, R. Colodner, S. Halachmi, E. Segal, Recent advances in the race to design a rapid diagnostic test for antimicrobial resistance, ACS Sens. 3 (2018) 2202–2217, https://doi.org/10.1021/acssensors.8b00900.
[2] Z.A. Khan, M.F. Siddiqui, S. Park, Current and emerging methods of antibiotic susceptibility testing, Diagnostics 9 (2019) 49, https://doi.org/10.3390/diagnostics9020049.
[3] J. Gao, L. Li, P.-L. Ho, G.C. Mak, H. Gu, B. Xu, Combining fluorescent probes and biofunctional magnetic nanoparticles for rapid detection of bacteria in human blood, Adv. Mater. 18 (2006) 3145–3148, https://doi.org/10.1002/adma.200601058.
[4] B. Jin, S. Wang, M. Lin, Y. Jin, S. Zhang, X. Cui, Y. Gong, A. Li, F. Xu, T.J. Lu, Upconversion nanoparticles based FRET aptasensor for rapid and ultrasenstive bacteria detection, Biosens. Bioelectron. 90 (2017) 525–533, https://doi.org/10.1016/j.bios.2016.10.029.
[5] S. Wu, N. Duan, Z. Shi, C. Fang, Z. Wang, Simultaneous aptasensor for multiplex pathogenic bacteria detection based on multicolor upconversion nanoparticles labels, Anal. Chem. 86 (2014) 3100–3107, https://doi.org/10.1021/ac404205c.
[6] C. Li, K. Vandenberg, S. Prabhulkar, X. Zhu, L. Schneper, K. Methee, C.J. Rosser, E. Almeide, Paper based point-of-care testing disc for multiplex whole cell bacteria analysis, Biosens. Bioelectron. 26 (2011) 4342–4348, https://doi.org/10.1016/j.bios.2011.04.035.
[7] H. Liu, F. Zhan, F. Liu, M. Zhu, X. Zhou, D. Xing, Visual and sensitive detection of viable pathogenic bacteria by sensing of RNA markers in gold nanoparticles based paper platform, Biosens. Bioelectron. 62 (2014) 38–46, https://doi.org/10.1016/j.bios.2014.06.020.
[8] A.B. Nurul Najian, E.A.R. Engku Nur Syafirah, N. Ismail, M. Mohamed, C.Y. Yean, Development of multiplex loop mediated isothermal amplification (m-LAMP) label-based gold nanoparticles lateral flow dipstick biosensor for detection of pathogenic Leptospira, Anal. Chim. Acta 903 (2016) 142–148, https://doi.org/10.1016/j.aca.2015.11.015.
[9] M.S. Verma, P.Z. Chen, L. Jones, F.X. Gu, "Chemical nose" for the visual identification of emerging ocular pathogens using gold nanostars, Biosens. Bioelectron. 61 (2014) 386–390, https://doi.org/10.1016/j.bios.2014.05.045.
[10] S. Nath, C. Kaittanis, A. Tinkham, J.M. Perez, Dextran-coated gold nanoparticles for the assessment of antimicrobial susceptibility, Anal. Chem. 80 (2008) 1033–1038, https://doi.org/10.1021/ac701969u.
[11] M.D. Adhikari, B.R. Panda, U. Vudumula, A. Chattopadhyay, A. Ramesh, A facile method for estimating viable bacterial cells in solution based on "subtractive-aggregation" of gold nanoparticles, RSC Adv. 2 (2012) 1782–1793, https://doi.org/10.1039/C1RA01023A.
[12] P. Nag, K. Sadani, S. Mukherji, S. Mukherji, Beta-lactam antibiotics induced bacteriolysis on LSPR sensors for assessment of antimicrobial resistance and quantification of antibiotics, Sensor. Actuator. B Chem. 311 (2020) 127945, https://doi.org/10.1016/j.snb.2020.127945.
[13] X. Zhang, X. Wang, Q. Yang, X. Jiang, Y. Li, J. Zhao, K. Qu, Conductometric sensor for viable Escherichia coli and Staphylococcus aureus based on magnetic analyte separation via aptamer, Microchim. Acta. 187 (2019) 43, https://doi.org/10.1007/s00604-019-3880-0.
[14] D.D. Galvan, Q. Yu, Surface-enhanced Raman scattering for rapid detection and characterization of antibiotic-resistant bacteria, Adv. Healthc. Mater. 7 (2018), e1701335, https://doi.org/10.1002/adhm.201701335.
[15] J. Plumbridge, E. Vimr, Convergent pathways for utilization of the amino sugars, Microbiology 181 (1999) 47–54.
[16] M.E. Olson, J.M. King, T.L. Yahr, A.R. Horswill, Sialic acid catabolism in Staphylococcus aureus, J. Bacteriol. 195 (2013) 1779–1788, https://doi.org/10.1128/JB.02294-12.
[17] R. Yokoyama, S. Itoh, G. Kamoshida, T. Takii, S. Fujii, T. Tsuji, K. Onozaki, Staphylococcal superantigen-like protein 3 binds to the Toll-like receptor 2 extracellular domain and inhibits cytokine production induced by Staphylococcus

aureus, cell wall component, or lipopeptides in murine macrophages, Infect. Immun. 80 (2012) 2816–2825, https://doi.org/10.1128/IAI.00399-12.
[18] C. Lee, P. Wang, M.A. Gaston, A.A. Weiss, P. Zhang, Plasmonics-based detection of virus using sialic acid functionalized gold nanoparticles, Methods Mol. Biol. 1571 (2017) 109–116, https://doi.org/10.1007/978-1-4939-6848-0_7.
[19] A. Jabłoński, K. Matczak, A. Koceva-Chyła, K. Durka, D. Steverding, K. Jakubiec-Krześniak, J. Solecka, D. Trzybiński, K. Woźniak, V. Andreu, G. Mendoza, M. Arruebo, K. Kochel, B. Krawczyk, D. Szczukocki, K. Kowalski, Cymantrenyl-nucleobases: synthesis, anticancer, antitrypanosomal and antimicrobial activity studies, Molecules 22 (2017), https://doi.org/10.3390/molecules22122220.
[20] G.I. Sakellari, N. Hondow, P.H.E. Gardiner, Factors influencing the surface functionalization of citrate stabilized gold nanoparticles with cysteamine, 3-mercaptopropionic acid or l-selenocystine for sensor applications, Chemosensors 8 (2020), https://doi.org/10.3390/chemosensors8030080.
[21] M.S. Sarwar, Q. Huang, A. Ghaffar, M.A. Abid, M.S. Zafar, Z. Khurshid, M. Latif, A smart drug delivery system based on biodegradable chitosan/poly(allylamine hydrochloride) blend films, Pharm. Times 12 (2020), https://doi.org/10.3390/pharmaceutics12020131.
[22] Z. Zhao, Q. Li, J. Gong, Z. Li, J. Zhang, A poly(allylamine hydrochloride)/poly (styrene sulfonate) microcapsule-coated cotton fabric for stimulus-responsive textiles, RSC Adv. 10 (2020) 17731–17738, https://doi.org/10.1039/d0ra02474k.
[23] V. Zucolotto, M. Ferreira, M.R. Cordeiro, C.J.L. Constantino, D.T. Balogh, A. R. Zanatta, W.C. Moreira, O.N. Oliveira, Unusual interactions binding iron tetrasulfonated phthalocyanine and poly(allylamine hydrochloride) in layer-by-layer films, J. Phys. Chem. B 107 (2003) 3733–3737, https://doi.org/10.1021/jp027573d.
[24] P. Singh, X. Ren, Y. He, L. Wu, C. Wang, H. Li, V. Singh, J. Zhang, Fabrication of β-cyclodextrin and sialic acid copolymer by single pot reaction to site specific drug delivery, Arab. J. Chem. 13 (2020) 1397–1405, https://doi.org/10.1016/j.arabjc.2017.11.011.
[25] M. Bou Khalil, M. Kates, D. Carrier, FTIR study of the monosialoganglioside GM1 in perdeuterated dimyristoylglycerophosphocholine (DMPCd54) multilamellar Bilayers: spectroscopic evidence of a significant interaction between Ca2+ ions and the sialic acid moiety of GM1, Biochemistry 39 (2000) 2980–2988, https://doi.org/10.1021/bi9923104.
[26] T. Elayabharathi, J. Vinoliya Josephine Mary, S. Mary Mettilda Bai, Characterization of a novel O-acetyl sialic acid specific lectin from the hemolymph of the marine crab, Atergatis integerrimus (Lamarck, 1818), Fish Shellfish Immunol. 106 (2020) 1131–1138, https://doi.org/10.1016/j.fsi.2020.07.039.
[27] N. Volz, J. Clayden, The urea renaissance, Angew. Chem. Int. Ed. 50 (2011) 12148–12155, https://doi.org/10.1002/anie.201104037.
[28] R.A. North, A.J.A. Watson, F.G. Pearce, A.C. Muscroft-Taylor, R. Friemann, A. J. Fairbanks, R.C.J. Dobson, Structure and inhibition of N-acetylneuraminate lyase from methicillin-resistant Staphylococcus aureus, FEBS Lett. 590 (2016) 4414–4428, https://doi.org/10.1002/1873-3468.12462.
[29] S. Link, M.A. El-Sayed, Size and temperature dependence of the plasmon absorption of colloidal gold nanoparticles, J. Phys. Chem. B 103 (1999) 4212–4217, https://doi.org/10.1021/jp984796o.
[30] C. Noguez, Surface plasmons on metal Nanoparticles: the influence of shape and physical environment, J. Phys. Chem. C 111 (2007) 3806–3819, https://doi.org/10.1021/jp066539m.
[31] C. Lee, M.A. Gaston, A.A. Weiss, P. Zhang, Colorimetric viral detection based on sialic acid stabilized gold nanoparticles, Biosens. Bioelectron. 42 (2013) 236–241, https://doi.org/10.1016/j.bios.2012.10.067.
[32] Y.G.Y. Chan, M.B. Frankel, D. Missiakas, O. Schneewind, SagB glucosaminidase is a determinant of Staphylococcus aureus glycan chain length, antibiotic susceptibility, and protein secretion, J. Bacteriol. 198 (2016) 1123–1136, https://doi.org/10.1128/JB.00983-15.
[33] O. Opota, K. Jaton, G. Greub, Microbial diagnosis of bloodstream infection: towards molecular diagnosis directly from blood, Clin. Microbiol. Infect. 21 (2015) 323–331, https://doi.org/10.1016/j.cmi.2015.02.005.
[34] P. Yagupsky, F.S. Nolte, Quantitative aspects of septicemia, Clin. Microbiol. Rev. 3 (1990) 269–279, https://doi.org/10.1128/CMR.3.3.269.
[35] A.D. Hay, K. Birnie, J. Busby, B. Delaney, H. Downing, J. Dudley, S. Durbaba, M. Fletcher, K. Harman, W. Hollingworth, K. Hood, R. Howe, M. Lawton, C. Lisles, P. Little, A. MacGowan, K. O'Brien, T. Pickles, K. Rumsby, J.A.C. Sterne, E. Thomas-Jones, J. van der Voort, C.A. Waldron, P. Whiting, M. Wootton, C. C. Butler, The Diagnosis of Urinary Tract infection in Young children (DUTY): a diagnostic prospective observational study to derive and validate a clinical algorithm for the diagnosis of urinary tract infection in children presenting to primary care with an acute i, Health Technol. Assess. 20 (2016) 1–197, https://doi.org/10.3310/hta20510.
[36] S. Müller, A.J. Wolf, I.D. Iliev, B.L. Berg, D.M. Underhill, G.Y. Liu, Poorly cross-linked peptidoglycan in MRSA due to mecA induction activates the inflammasome and exacerbates immunopathology, Cell Host Microbe 18 (2015) 604–612, https://doi.org/10.1016/j.chom.2015.10.011.
[37] N. Mistretta, M. Brossaud, F. Telles, V. Sanchez, P. Talaga, B. Rokbi, Glycosylation of Staphylococcus aureus cell wall teichoic acid is influenced by environmental conditions, Sci. Rep. 9 (2019) 3212, https://doi.org/10.1038/s41598-019-39929-1.
[38] B. Khatua, A. Ghoshal, K. Bhattacharya, C. Mandal, B. Saha, P.R. Crocker, C. Mandal, Sialic acids acquired by Pseudomonas aeruginosa are involved in reduced complement deposition and siglec mediated host-cell recognition, FEBS Lett. 584 (2010) 555–561, https://doi.org/10.1016/j.febslet.2009.11.087.
[39] G.H. Thomas, Sialic acid acquisition in bacteria-one substrate, many transporters, Biochem. Soc. Trans. 44 (2016) 760–765, https://doi.org/10.1042/BST20160056.
[40] X. Yang, Y. Dang, J. Lou, H. Shao, X. Jiang, D-alanyl-D-alanine-modified gold nanoparticles form a broad-spectrum sensor for bacteria, Theranostics 8 (2018) 1449–1457, https://doi.org/10.7150/thno.22540.
[41] L. Zhu, S. Li, X. Shao, Y. Feng, P. Xie, Y. Luo, K. Huang, W. Xu, Colorimetric detection and typing of E. coli lipopolysaccharides based on a dual aptamer-functionalized gold nanoparticle probe, Microchim. Acta. 186 (2019) 6–11, https://doi.org/10.1007/s00604-018-3212-9.
[42] C. Shin, H.N. Lee, J.S. Ryu, H.J. Chung, Rapid naked-eye detection of Gram-positive bacteria by vancomycin-based nano-aggregation, RSC Adv. 8 (2018) 25094–25103, https://doi.org/10.1039/c8ra03540g.